

Methodology for creating and calibrating DFN models from digital terrain models in underground mining, Chuquicamata underground case study

C. Divasto^a, G. Barindelli^b and J. Pereira^a

^a*DERK Ingeniería y Geología Ltda., Calama, Chile*

^b*GRMD División Chuquicamata de Codelco Chile, Calama, Chile*

ABSTRACT

The acquisition of structural data for purposes of geometrical modelling of rock masses in underground works entails inherent difficulties given the density of structural data required, spatial limitations of mine workings, the safety standards compliance, and operational requirements that reduce the exposure time of bare rock in headings before the implementation of fortification. This work presents a methodology for the development of Discrete Fracture Network (DFN) models with a focus on underground mining usage. As an alternative to field mapping, virtual mapping methods of Digital Terrain Models (DTM) generated with photogrammetric techniques were applied. The workflow includes 4 main stages; (1) the first stage is associated with the generation of DTM with photogrammetric technology; (2) the second stage develops the capture of the fracture's structural information focused on the geometric description of joints (orientation and persistence); (3) the third stage involves the processing of sampled data, identifying joint's data sets, discontinuity density (P10) and finally, discontinuity's trace length distribution applying the concept of fracture's fractal behavior; (4) finally, the fourth stage consider the construction of DFN models and their calibration with respect to the previously defined structural parameters, this stage is carried out using WSP-Golder's FracManTM commercial software. Also, an adjustment factor to incorporate borehole data is proposed. The methodology is applied to the Block Caving project Chuquicamata Underground Mine in Chile. The results show the influence of fractures persistence and scale effect on the fragmentation.

1 INTRODUCTION

Chuquicamata Underground Mine is a copper-molybdenum Mine located in the Codelco Norte Division in Calama, north of Chile, its extraction began in 2019 as a block caving project. One of the most important factors in a caving process corresponds to rock mass fragmentation because a good prediction about fragmentation entails to better rock mass characterization, subsidence, and hang up prediction analysis, which in turn will contribute to determining design factors, preconditioning and the operation (Ortiz, 2018).

Discrete Fracture Networks model (DFN) is a specific modelling methodology that tries to describe and replicate the fractures of a rock mass through the simulation of discrete

discontinuities whose geometrical properties, such as, orientation, frequency, and persistence are defined by probability density functions (PDF) based on field mapping or core logging. In that way, a good DFN model could be used to estimate the degree of rock mass fracturing (Rogers et al, 2010; Ortiz, 2019; Guajardo et al, 2022), evaluate the probability of unstable blocks (Rogers et al., 2006; Rogers et al., 2016; Divasto, 2018), characterize the rock mass (Elmo et al., 2014), model hydrogeological flows (Rogers et al., 2009), define and evaluate mining design (Hekmatnejad et al., 2022; Kuppusamy, 2022), among others. Nevertheless, the construction of a DFN requires that the input data fulfill some minimal requirements of quality and quantity information to define the

geometrical variables with the support the statistics.

In the Chuquicamata Underground mine, the acquisition of structural information from field mapping of drifts entails some difficulties which are associated with limited exposure time of bare rock in headings before the implementation of fortification, safety standards that restrict exposure of people in unfortified areas and scale limitations which imply sampling biases.

Because of the limitations stated above, this work proposes a DFN construction methodology that focuses on the sampling and analysis of discontinuity data derived from photogrammetric models, which are generated routinely as a backup of the rock mass characterization. This methodology is proposed as a complementary work activity to *in situ* mapping in underground mines.

Moreover, we seek to apply this methodology to estimate the granulometric curves of In Situ Fragmentation by adding core logging information near the area of interest. Additionally, we try to evaluate the approach proposed by Cai et al. (2004) about the effect of fracture lengths and rock bridges on fragmentation at different observation scales.

In this work joint, fracture, and discontinuity are used with the same interchangeably.

2 GEOLOGICAL SETTING

Chuquicamata Underground is situated in the Precordillera of the Atacama Desert, west of the modern volcanic arc of the Andean Range. It is a copper-molybdenum porphyry deposit related to intrusive magmatism of the Eocene – Oligocene age (Maksaev et al., 1988, Maksaev, 1990 in Siña et al., 2005). This mega deposit is part of the metallogenic province from Upper Eocene – Lower Oligocene, which is aligned with the Domeyko Fault System from Quebrada Blanca – Collahuasi to Potrerillo – El Salvador (Siña et al., 2005).

The ore body of Chuquicamata is elongated in the NNE-SSW direction, with 4 km in length and 300 m to 900 m in width, being narrower southwards. The predominant geological unit is

the Chuquicamata Intrusive Complex which occurs as a mega subvertical dyke and is limited on its western side by the West Fault, and eastward by the Mesabi Fault or East Deformation Zone. The Complex is divided into three main intrusive bodies, Pórfido Este, Pórfido Blanco, and Pórfido Oeste whose compositions range from granodiorite to quartz monzodiorite rock types. The Pórfido Este contains most of the metallic mineralization with economic benefits, with the greatest grades hosted in zones of structural weakness (Espinoza, 2018).

Regarding hydrothermal alteration, the Chuquicamata Complex consists of a huge volume of background potassic alteration with more intense zones, which are overprinted by a younger phyllic alteration of pyrite-sericite (Rivera et al., 2012). It has been proven that the injection of copper into the hydrothermal system has been due to early mineralization events, but the highest hypogene grades occur in zones with late quartz-sericite alteration which in turn obliterate the early alteration associations (Codelco Norte, 2009).

Concerning Structural Domains, Chuquicamata Underground is mainly placed in the Americana Domain. This domain is characterized by being flanked on its western side by the West Fault and on its eastern side by the Americana Fault. In turn, the Americana Domain is subdivided into three sub-domains denoted as: Americana North, Central, and South, respectively, which are defined by trend breaks of Barton's NGI-Q parameter (Barton et al., 1974) value distributions (Codelco Norte, 2009).

The concept of Basic Geotechnical Units (UGTB initials in Spanish) has been developed for the geotechnical characterization of Chuquicamata Mine. It consists of relatively homogeneous bodies of rock mass that result from the superimposition of Alteration Geological Units onto the Lithological Units, restricted to the mineralization zone. Thirteen UGTBs has been identified, of which the main ones are Roca Cuarzo Sericita (RQS), Pórfido Este Sericítico (PES), and Pórfido Este Potásico (PEK).

The RQS UGTB results from the superposition of Quartz- Sericite Alteration over the Lithological Unit Pórfido Este. This unit is defined as a strongly altered rock, with quartz as the main mineral which is observed as recrystallized grains or like polydirectional veinlets, in a fine aggregate of sericite and alteration clays. This geotechnical unit has an important variability in its geotechnical quality, associated with the percentage of quartz and sericite. There are three distinctive subunits named Cuarzo Igual Sericita (QIS), Cuarzo Mayor Sericita (QMS) and Cuarzo Menor Sericita (QMES) (Espinoza, 2018).

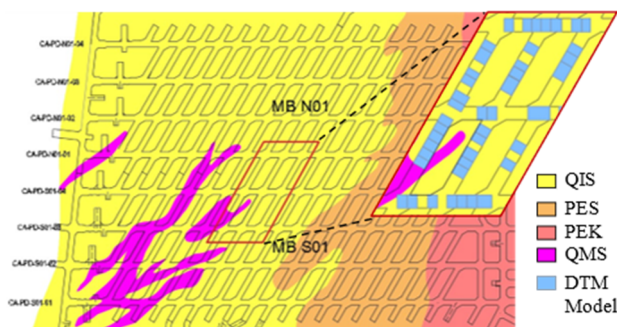


Figure 1 UGTB model of the study area, MBC N01-S01. Additional Close-up view with DTM models used for mapping.

Table 1 UGTB QIS Properties (Díaz et al., 2018)

UGTB	Density (t/m^3)	UCS (MPa)	TS (MPa)	E (GPa)	GSI
QIS	2.70	66	-2.0	20	62(54-70)

UCS: Uniaxial Compressive Strength, TS: Traction Strength, E: Young's Modulus, GSI: Geological Strength Index.

The area of study included in this work mainly comprises the QIS unit (see Figure 1). In general terms, this subunit is described as an altered rock composed of secondary quartz and sericite, which occur in a penetrative mode, obliterating the original rock texture in its entirety. Anhydrite crystals and minor quantities of gypsum are also recognized. Its main characteristic is the quartz content, and complementary sericite content, with a percentage between 30% to 60% of the

rock. The geotechnical properties are summarized in Table 1.

3 METHODOLOGY AND INPUT DATA

In this section, there will be a description in detail of the steps applied in the development of DFN models, procedures, and theoretical fundamentals on which this methodology is based. Additionally, the data obtained in each stage of the methodology is presented simultaneously.

3.1 Digital Terrain Model Acquisition

The first stage consists of the process of Digital Terrain Models (DTM) construction, which is generated by photogrammetry surveying. This step requires a high standard of procedures that allows to the creation of qualified and georeferenced DTM models, while they form the basis of the following processes.

Chuquicamata Underground Mine has incorporated this process to survey the tunnels and as backup information. The sequence of activities commences with the drifting process, after each blasting event, the mine operations team is responsible for gas evacuation, muck movement, scaling of unstable blocks, cleaning, and heading availability for the surveying personnel.

The surveying team oversees the marking of reference points, light focus placing, and installing the stations from where the photos will be taken. Each element must be positioned with a specific distribution, taking care of the distance between control points, linearity of stations, and directionality of light focuses, to avoid shadows and light intensity changes. Every captured information is stored in a digital platform for processing (Figure 2) (González, 2022).

Each DTM project must contain a set of 16 photos and a text file with the coordinates of control points. The files are processed by a specialist technician using the 3DM Analyst Mine Mapping Suite software (ADAM Technology, 2024). The outcome of the process corresponds to a set of files ready to be used by different users.

Finally, for this study, the files are reprocessed to cloud points data using the open-source

project Cloud Compare v2.13 (CloudCompare, 2023).

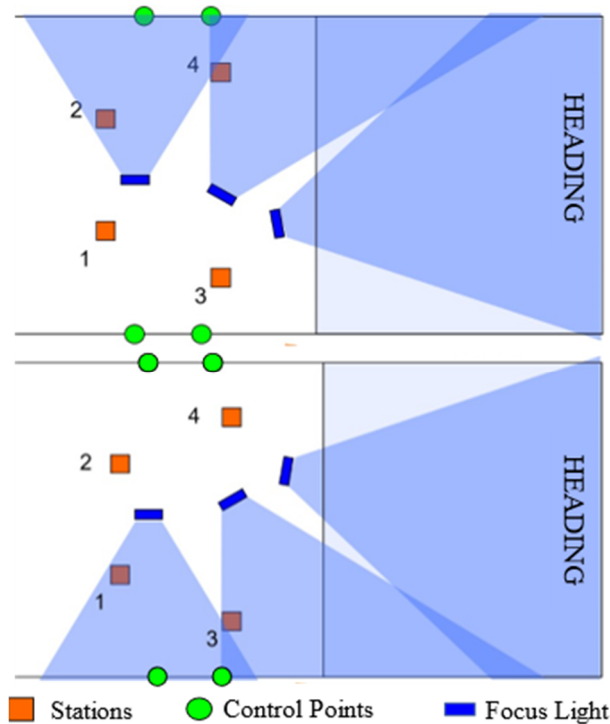


Figure 2 Schematic diagram to show to capture the photos.

3.2 Discontinuity Mapping in DTM

The fracture sampling process is essential for DFN model construction, not only because of the amount of data accumulated but also due to the sampling method applied. Such will define the scopes and biases of the geometrical properties of the discontinuities.

The main biases to which fracture sampling is subjected in two-dimensional outcrops have been described in the literature. Mauldon & Dershowitz (2000) identify them as sampling problems denoted as: i) censoring, which depends on the resolution of the DTM (in this case) and mapping scale, which mainly affects to small fractures, ii) length-bias, explained by the greater probability to sample long discontinuity compared to small ones, iii) truncation, type of bias that the intrinsic limitation of a tunnel given its size, so the fractures are truncated towards the edge of the excavation; and finally v) orientation bias, which depends on the occurrence probability of a discontinuity in an outcrop because of its

orientation, similar to the Terzaghi effect (Terzaghi, 1965).

A variety of well-known fracture sampling techniques have been applied and used such as scanline sampling, circular scanline sampling, and window sampling (Zeeb et al., 2013). Each of them has pros and cons regarding mapping biases and hence geometrical aspects that are required to solve.

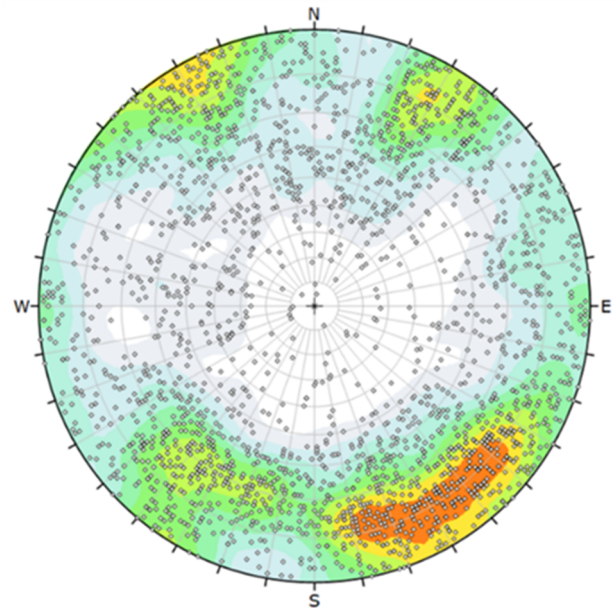


Figure 3 Contour plot of 2297 discontinuities sampled from the DTM models.

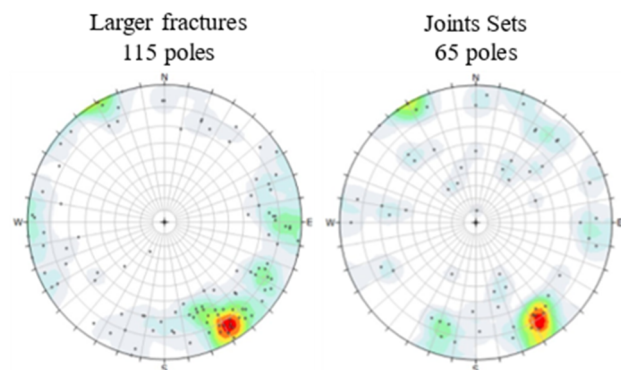


Figure 4 Contour plot of previously mapped discontinuities sampled from fieldwork.

In this work, the capture of discontinuities was executed with the software Point Studio v8.1 (Maptek, 2019). The sampling was developed through integrated windows sampling since the DTM models were available where it is possible to observe at the same time the lateral and front

walls outcrops, even the roof of the excavation, so fractures can be sampled through all these sections. This method reduces but does not eliminate some biases, such as orientation and truncation biases. Regarding censoring, the models were adjusted according to Point Cloud density, which is its resolution, however, a minimum limit of trace fracture was defined, which is about 20 to 25 cm. Lastly, to statistically reduce the effect of length bias, a procedure defined by La Pointe (2002) was applied, explained later.

38 DTM models were processed in total, and the number of fractures mapped was 2297, without doing a distinctive structural classification between them. Figure 3 shows a contour plot with fracture poles included. This information was compared with previously mapped discontinuities from the routinary fieldwork of the study area which only focuses on larger fractures that may have an importance in the structural control of the tunnel, and an identification of discontinuity sets (Figure 4).

3.3 Discontinuity Processing and Analysis

In this section a statistical analysis is made of the information previously collected, the main objectives are: (1) identifying joint sets that control the block geometry, (2) measuring spacing and fracture frequency (FF) of each set defined, and (3) determining fracture radius distribution from trace length mapped of each set.

3.3.1 Fracture sets identification

The identification of a joint data set was developed through contour plot analysis using Dips v7.0 software (Rocscience, 2019). Considering that the study area is located inside the same Structural Domain (Subdomain Americana Central) and that the geotechnical unit QIS is the most predominant, the information was analyzed as a single data set.

There were four structural sets defined, (see Figure 5). Note that sets 1a and 1b, 2a and 2b, and 3a and 3b, all of them sub-verticals, were assigned as single sets for practical purposes of analysis and modelling. While the fourth set was

defined as inclined to sub-horizontal, despite not being identified. The latter had the purpose of incorporating those fractures that were not represented in the diagram plot into the DFN model, possibly due to bias surveying. The information of each set is summarized in Table 2

3.3.2 Spacing and fracture frequency

Once the structural sets are defined, the next step consists of determining the mean spacing and its associated fracture frequency. To achieve this goal an algorithm within the Point Studio software was applied.

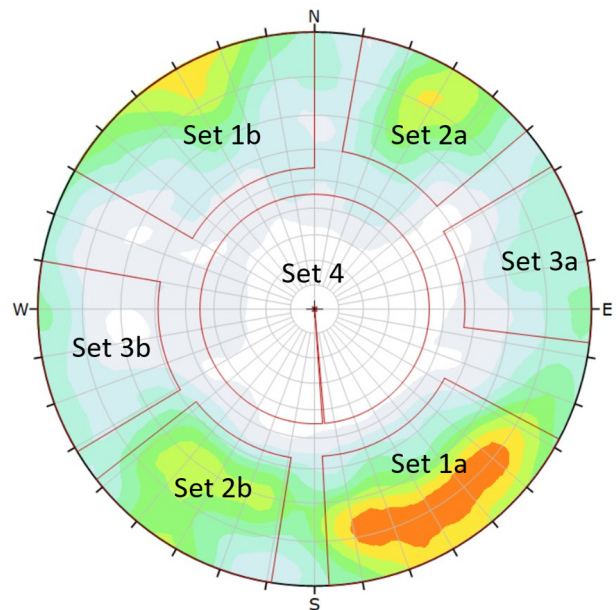


Figure 5 Fracture Sets identification in contour Plot.

Table 2 Mean Structural Sets orientation

Structural Set	Dip (°)	DipDir (°)	N° Polos
Set 1	86	329	893
Set 2	86	30	538
Set 3	90	264	340
Set 4	11	136	175

First all fracture sets must be separated from each other, then it is required that evaluation zones must be designated, and each zone must meet the requirement of mapping continuity (the gaps between DTM separate different zones). Afterwards, the spacing algorithm is applied to

the different zones for each fracture set. This algorithm estimates the mean orientation of the selected data to interpolate a new structural disc replacing the original fracture, an extrapolation of fracture length can be defined if it is necessary, and finally, the algorithm draws perpendicular lines between adjacent fractures, which represents the spacing among joints (see Figure 6).

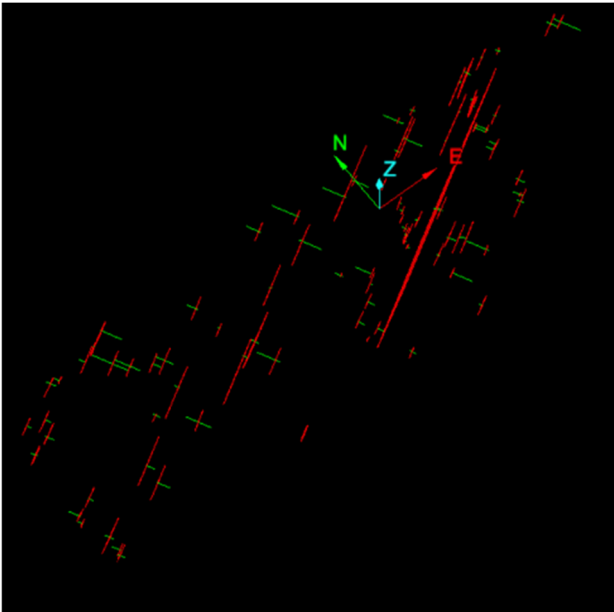


Figure 6 Perspective view of a set spacing estimation.

Table 3 UGTB QIS fracture spacing

Set	Mean Spacing (m)	Mean Fracture Frequency (1/m)
Set 1	0.24	4.1
Set 2	0.67	1.5
Set 3	0.77	1.3
Set 4	0.66	1.5

This process was applied to each structural set; furthermore, a 2.5 m extrapolation was considered for every fracture as a more conservative strategy to link a higher number of fractures. The results of this evaluation are indicated in Table 3, where information about mean spacing and mean fracture frequency is presented.

3.3.3 Length discontinuity distribution

This analysis is supported by fractal geometry of discontinuities, which can be understood as a geometric similarity at independent scales (Push, 1995). La Pointe (2002) applies this concept and then characterizes it with a Power Law equation (Equation 1), where $G(x)$ is the Complementary Cumulative Density Function (CCDF), X_0 is the minimum radius size, X is any fracture with a size within X_0 and infinite, and D is the exponent of fractal dimension.

$$G(x) = \left(\frac{x_0}{x}\right)^D \quad (1)$$

Therefore, a Power Law plot of the CCDF of a fracture radius data set represents the fractal behavior of joints, whose slope indicates the fractal dimension exponent (D).

Additionally, La Pointe (2002) resolves the correlation between fracture radius distribution and trace length distribution formed when fracture discs intersect a surface. Equation 2 shows the relationship between D and D' factors, which are the exponents of fracture radius distribution and trace lengths distribution, respectively.

$$D = D' + 1 \quad (2)$$

This methodology was applied to the trace length data of each joint set, and then the slope of every graph was identified and consequently the fractal dimension factor D' . In Figure 7 the CCDF plots of each fracture set can be observed and its respective D' factor.

3.4 DFN Model Calibration

The referred information is integrated to simulate the DFN models, using the FracMan™ software of WSP-Golder (Golder, 2021). To generate a DFN model some basic parameters must be input, these are: the spatial location of fracture discs, the orientation of joints, intensity (see Figure 8), and persistence of trace length. Each of these parameters is defined by a Probability Distribution Function (PDF).

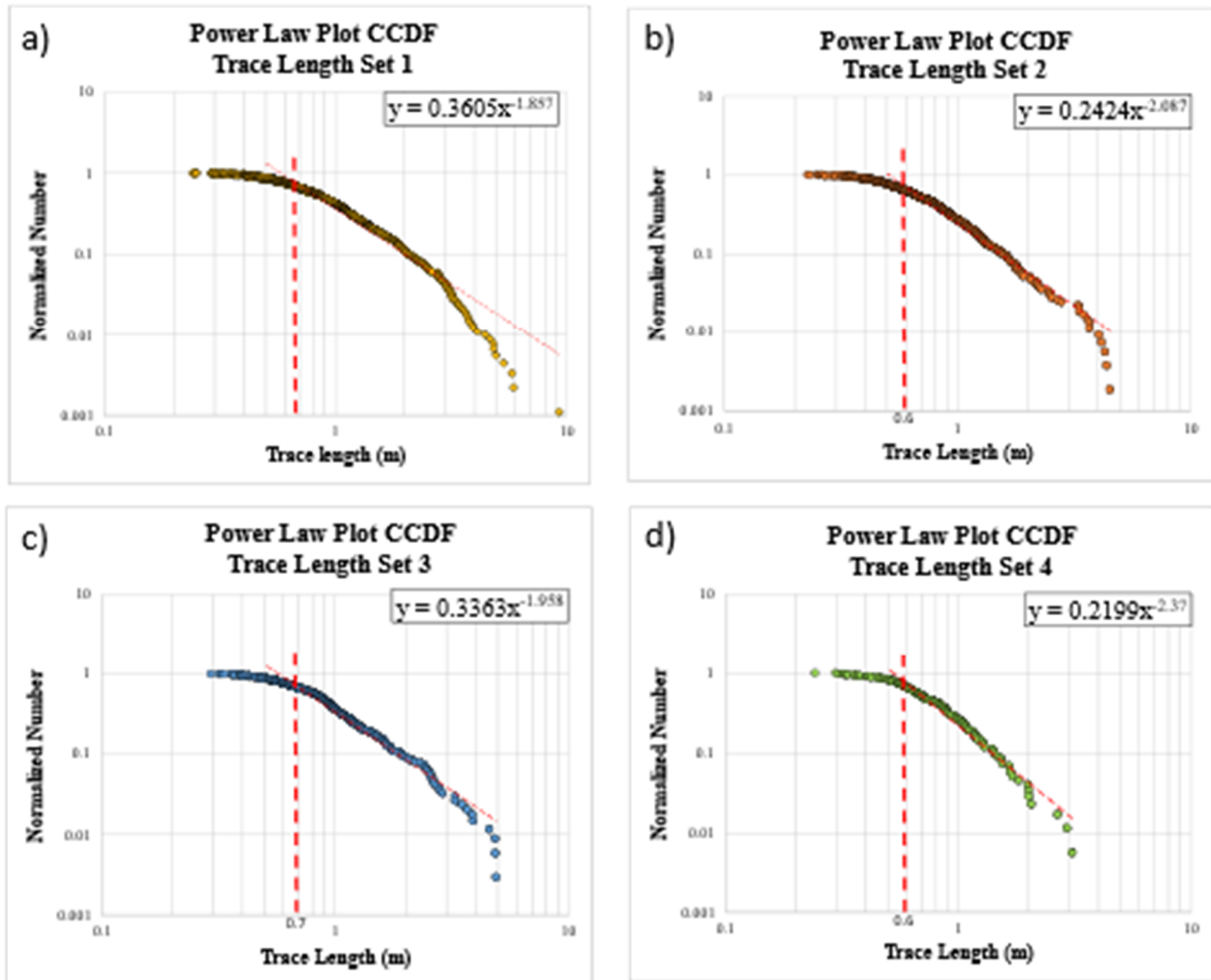


Figure 7 CCDF Plot of each fracture Set with its respective D' factor.

Dimension of sampling region	Dimension of feature				
	0	1	2	3	
0	P_{00} N° of fractures per point sample				Point Measures
1	P_{10} N° of fractures per unit length	P_{11} Length of fractures per unit length			Linear Measures
2	P_{20} N° of fractures per unit area	P_{21} Length of fractures per unit area	P_{22} Area of fractures per unit area		Area Measures
3	P_{30} N° of fractures per unit volume	P_{31} Length of fractures per unit volume	P_{32} Area of fractures per unit volume	P_{33} Volume of fracture per unit volume	Volumetric Measures
	Density		Intensity	Porosity	

Figure 8 Intensity measure types of fractures (modified by Mauldon & Dershowitz, 2000).

In this work, the location of the discs which are evidenced as fractures is resolved according to the Enhanced Baecher distribution model, which places uniformly the center of each disc into space using Poisson processes (Golder, 2021).

The orientations of joint sets were solved with the Bootstrapping method, which replicates statistically the fracture poles concentration, where a k constant equal to 200 was applied to reduce the dispersion of each simulated set.

On the other hand, the intensity value was analyzed with the P_{10} (fracture frequency) and P_{32} (area of fractures per unit volume) parameters, its correlation is indicated in Equation 3, proposed by Dershowitz & Herda (1992), whose C_{31} factor is solved through simulations of all fracture sets individually, because it depends on the geometric characteristics of each one.

$$P_{32} = C_{31} * P_{10} \quad (3)$$

Ultimately, the fracture's trace length was plotted in Power Law graphs to obtain the D' factor as was explained in the previous section.

The validation and calibration of these geometric parameters are indicated below.

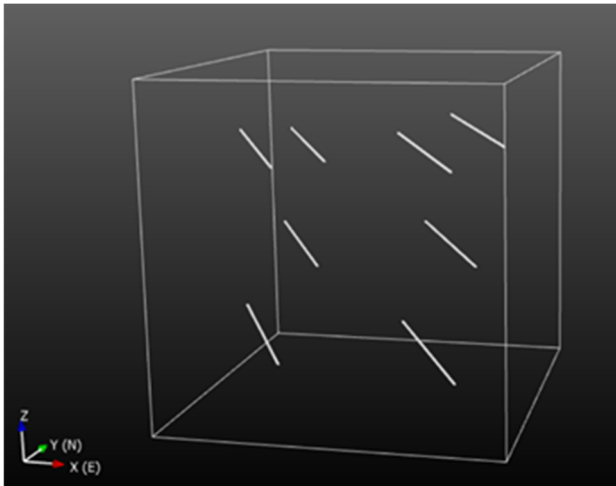


Figure 9 Perspective view of simulated boreholes inside evaluation box.

3.4.1 Intensity calibration and validation

The main element to measure the fracture intensity was the P_{10} variable. This parameter is commonly measured in core logging, as well as, during outcrops mapping of tunnels when

describing joint sets. The validation of this variable was realized with an empirical method through simulations of DFN and boreholes, these boreholes were modeled as cylinders of 20 m long and with a radius of 3 cm, whose orientations were orthogonal to each fracture set. There were considered 8 simulated boreholes to every joint set, aleatory distributed in an evaluation box of 40 m sides (see Figure 9).

The simulation method consists of an evaluation of a DFN model with a known P_{32} intensity, through the intersection of the simulated boreholes and the DFN model estimates the FF in each borehole, then a mean P_{10} value is defined. Applying Equation 3 can the C_{31} constant can be calculated that is unique for each data set. With this, any P_{32} estimation can be done directly from the P_{10} and C_{31} variables. The advantage of P_{32} is that it is scale-independent so the same value can be applied to different volumes of analysis.

Table 4 Discontinuous Model Intensity

Parameter of Intensity	Discontinuous Model			
	Set 1	Set 2	Set 3	Set 4
P_{10} (1/m)	4.10	1.50	1.30	1.50
C_{31}	0.96	0.84	0.87	0.86
P_{32} (m ² /m ³)	3.94	1.26	1.13	1.28

Table 5 Continuous Model Intensity

Parameter of Intensity	Continuous Model			
	Set 1	Set 2	Set 3	Set 4
P_{10} (1/m)	4.10	1.50	1.30	1.50
C_{31}	1.06	1.04	1.00	1.10
P_{32} (m ² /m ³)	4.33	1.57	1.29	1.66

This procedure was applied to each fracture set; however, two different scenarios were considered. The first, called the Discontinuous Model, considers the fractal distribution to solve fracture trace length, while, the second scenario called the Continuous Model, assumes a long enough persistence of fractures to cross the volume of analysis. Table 4 and Table 5

summarize the results obtained for every fracture set in the Discontinuous and Continuous Models, respectively.

3.4.2 Fracture orientation validation

Once the fracture intensity is calibrated, it is possible to assess if a contour plot from the DFN complies with the original fracture pole dispersion. In this step three DFN simulations were computed, all of them with the four fractures sets included, the global P_{32} (sum of P_{32} of each set) was assigned as 1, 5, and 11 (m^2/m^3) values. The result of the calibration is observed in Figure 10, which compares the different contour plots.

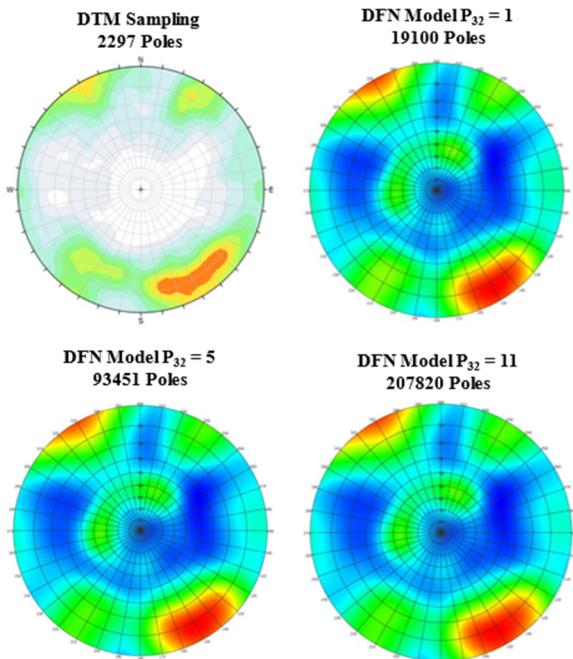


Figure 10 Contour Plots comparison among the DFN simulations and the original fracture mapping.

3.4.3 Persistence validation

This section aims to validate the methodology used to identify the fracture radius distribution. The procedure applied makes use of DFN models with a known D' factor and is restricted to one fracture set orientation. In addition, different surfaces were simulated within the evaluation box of 40 m sides, which served to represent the walls of an excavation. Three different cases were considered.

Case 1. Evaluate the scale effect, simulating different surfaces of 25 m^2 , 100 m^2 , 400 m^2 and 1600 m^2 (see Table 6).

Table 6 Case 1, expected D' factor 1.58

Area (m^2)	Mapping Cells	D' Factor			
		Mean	Min	Max	Std Dev
25	8	1.51	1.07	1.74	0.26
100	8	1.48	1.33	1.60	0.09
400	8	1.54	1.46	1.65	0.07
1600	4	1.60	1.55	1.65	0.04

Case 2. Evaluate the orientation effect, integrating cells with different trends, trying to simulate the Production Drifts and Draw Point Drifts. Specifically, there were four defined main trends, named, lateral production drift (LPD), front production drift (FPD), lateral draw drift (LDD), and front draw drift (FDD). See Table 7 for results.

Table 7 Case 2, expected D' factor 1.85

Code	Mapping Cells	D' Factor			
		Mean	Min	Max	Std Dev
LPD	4	1.80	1.76	1.82	0.03
FPD	4	1.81	1.75	1.84	0.04
LDD	4	1.78	1.74	1.80	0.03
FDD	4	1.71	1.64	1.81	0.08

Case 3. It simulates the shape of a tunnel and the effect of fractures intersecting the width of the entire excavation, instead of a simple wall side. Figure 11 shows a plot of the CCDF function of all fracture traces identified in the simulation. Additionally, the D' factor is presented.

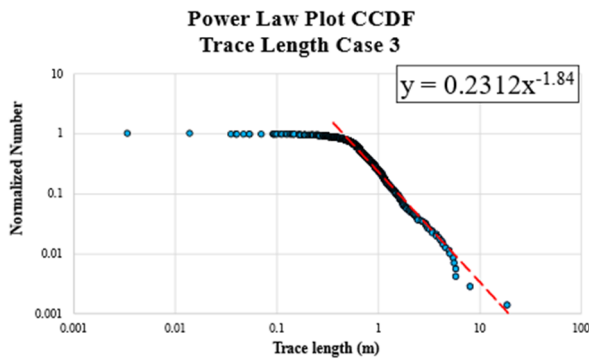


Figure 11 Case 3 expected D' factor 1.86.

3.5 Integrating Core Logging Information

The methodology described above allows to generate calibrated DFN models according to the geometrical characteristics identified during fracture mapping with the Digital Terrain Models. Nevertheless, sometimes the main information source in underground mining projects comes from core logging, and preliminary engineering designs are evaluated with this information. Because of that, it is proposed to complement the information that will be used to develop the fragmentation analysis derived from DFN models, by integrating in the process the information from core logging near the study area.

As a reference the methodology proposed by Guajardo & Russo (2021) is considered. This method transforms the FF parameter measured from cores into the P_{32} variable of each measurement tract, obtaining a histogram of intensity frequencies. This represents the variability of fracturing in the rock mass. To unify and compare the two sources of information, an adjustment factor named Terzaghi Adjustment Factor (TAF) is proposed. Such allows the integration of core logging data as well as the transformation of the linear intensity parameter P_{10} into the volumetric intensity parameter P_{32} reducing the orientation bias.

3.5.1 Terzaghi adjustment factor

To compare the FF parameter from core logging data with the information captured in digital mapping it was necessary to resort to the Terzaghi Correction proposed by Terzaghi (1965). This is expressed as indicated in

Equation 4, where FF is the real fracture frequency, FF' the apparent fracture frequency and α the angle between a joint set and the borehole.

$$\frac{FF'}{FF} = \sin \alpha \quad (4)$$

Four boreholes with fracture frequency data were identified near the study area (see Figure 12). The information from each borehole is presented in Table 8.



Figure 12 Boreholes near the area of study. MBC N01-S01.

Table 8 Borehole Characteristics

Borehole	Collar (m)			Orientation		Length (m)
	East	North	Height	Trend (°)	Plunge (°)	
CHDD 10250	3163	3864	1847	211	7	195
CHDD 10241	3162	3869	1846	360	13	165
CHDD 10249	3164	3868	1846	315	65	315
CHDD 8623	3165	3864	1850	100	64	270

The angle between the mean orientation of each set and boreholes is denoted as, α_t , (see Table 9).

Furthermore, Table 10 shows the inverse value of $\sin(\alpha_t)$ of every single angle to have a better perspective of the Terzaghi Correction.

Table 9 Angle between Sets and boreholes

Structural Set	α_t Set – Borehole (°)			
	CHDD 10250	CHDD 10241	CHDD 10249	CHDD 8623
Set 1	29	55	20	21
Set 2	87	55	2	5
Set 3	37	6	15	26
Set 4	4	20	76	55

Table 10 Original Terzaghi Factor

Structural Set	Original Terzaghi Factor			
	CHDD 10250	CHDD 10241	CHDD 10249	CHDD 8623
Set 1	2.1	1.2	3.0	2.8
Set 2	1.0	1.2	23.4	10.9
Set 3	1.7	9.5	3.9	2.3
Set 4	13.5	2.9	1.0	1.2

Table 11 Theoretical FF' Estimation

Structural Set	Theoretical FF' estimation (1/m)			
	CHDD 10250	CHDD 10241	CHDD 10249	CHDD 8623
Set 1	2.0	3.4	1.4	1.5
Set 2	1.5	1.2	0.1	0.1
Set 3	0.8	0.1	0.3	0.6
Set 4	0.1	0.5	1.5	1.2

When applying Equation 4 is possible to deduce the apparent fracture frequency (FF') of each joint set to every borehole orientation (see Table

11). This is a necessary step to understand the expected relative percentage of the different sets in each evaluation trend.

Terzaghi (1965), indicates that there isn't an adequate correction to low values of α because, in a rock mass the number of fracture intersections is significantly affected by local variability of discontinuity in terms of spacing and fracture length. Likewise, the variability of discontinuity sets orientation also has an impact on the quantity of intersections.

Table 12 Simulated FF' Estimation

Structural Set	Simulated FF' Estimation (1/m)			
	CHDD 10250	CHDD 10241	CHDD 10249	CHDD 8623
Set 1	2.0	3.5	1.8	2.0
Set 2	1.3	1.3	0.5	0.6
Set 3	0.8	0.4	0.6	0.7
Set 4	0.7	0.7	1.4	1.1

Table 13 Simulated Terzagui Factor

Structural Set	Simulated Terzagui Factor			
	CHDD 10250	CHDD 10241	CHDD 10249	CHDD 8623
Set 1	2.0	1.2	2.3	2.1
Set 2	1.2	1.2	3.2	2.6
Set 3	1.6	3.0	2.3	1.9
Set 4	2.0	2.1	1.1	1.3

To overcome this situation, an empirical solution was necessary making use of DFN models. A DFN of every discontinuity set was simulated in a standard box of 40 m sides. Additionally, cylinders were created of about 20 m length to recreate the boreholes near the study area. Subsequently, the apparent fracture frequency was measured for every set in each borehole, resulting in Table 12. Then, applying Equation 4 to these results, it is possible to get a Simulated

Terzaghi Correction (Table 13), which represents the geometrical variability of a DFN model.

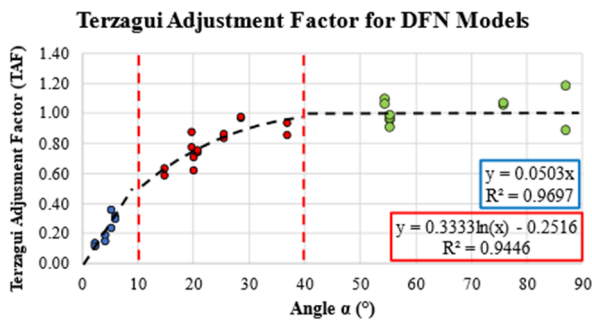


Figure 13 Terzaghi Adjustment Factor Plot.

$$y = 0.0503x \quad (5)$$

$$y = 0.333 \ln x - 0.2516 \quad (6)$$

The ratio between the simulated Terzaghi Correction and the original Terzaghi Correction was defined as the Terzaghi Adjustment Factor (TAF) and was plotted against the angle α (Figure 13). It resulted in a correlation curve where the TAF value trended to 1 when α trend to 90° . Thereby, it was possible to define an adjustment to the Terzaghi Correction depending on the angle of intersection α . The application of TAF is limited to this study with the characteristics applied to DFN models.

Table 14 Modified Terzagui Factor

Structural Set	Modified Terzagui Factor			
	CHDD 10250	CHDD 10241	CHDD 10249	CHDD 8623
Set 1	1.8	1.2	2.2	2.1
Set 2	1.0	1.2	2.9	2.9
Set 3	1.6	2.9	2.5	1.9
Set 4	2.9	2.2	1.0	1.2

The correlation curve in Figure 13 was subdivided into three main sections to facilitate the analysis: the first section defined by Equation 5, ranges from 0° to 10° degrees, and a linear correlation was applied; between 10° and 40° degrees a logarithmic correlation was

applied (Equation 6); and between 40° and 90° degrees the TAF value was kept constant as 1.

Table 14 shows the modified Terzaghi Correction which includes the TAF adjustment. Consequently, the analysis of core logging was processed with this new correction.

3.5.2 Fracture frequency analysis from boreholes

The procedure of core logging in Chuquicamata Underground includes composites or sections of 3 m to capture the information. Regarding the information of interest for this study, each section contains the number of intersecting fractures and categorization according to the characteristics of filling minerals and fracture aperture. The classification is described below: Joints (discrete fractures with no filling, or with very thin coating), JCA (opened discontinuities with a regular filling, usually soft minerals), JCC (closed discontinuities with hard fillings) and Soft Vein (closed discontinuities of soft fillings). Unfortunately, the boreholes considered for evaluation only included information on Joints, JCA, and JCC, making no distinction between JCC and Soft Veins, therefore, only the Joints and JCA were considered to estimate the fracture frequency per section.

The transformation of the FF' parameter of each section to P_{32} entails the following sequence: first a comparison table must be created; this table is obtained from the P_{10} estimated from digital mapping which is transformed to an FF' through the application of Equation 4 with the data of Table 14. Then, comes the processing of core logging, which depends on the apparent fracture frequency (global FF') observed in every composite (sections of 3 m); therefore, to know the number of fractures that correspond to a different set, the global FF' must be recalculated in proportion to the previous estimation of the FF'. Subsequently, the new weighted FF' is transformed to FF or P_{10} applying Equation 4. Finally, the C_{31} constant is applied to transform the P_{10} value to P_{32} .

The sum of these values indicates the global volumetric intensity of a composite or section. Consequently, considering all data from the

analyzed sections a histogram was made, which represents the variability of the fracture intensity in a rock mass and therefore its fragmentation.

The histogram created contains ranges of P_{32} intensity. Each range is worked as an independent DFN model and, therefore, as an independent granulometric curve. Considering the weighting of every range from the histogram, a global granulometric curve can be obtained, which is representative of the evaluated rock mass.

Figure 14 and Figure 15 show the weighted frequency histogram of P_{32} intensity obtained from Joints and JCA from core logging, for the Discontinuous and Continuous Model, respectively.

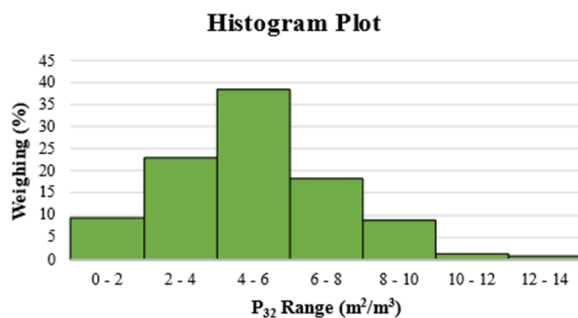


Figure 14 Histogram of P_{32} parameter from boreholes, Discontinuous Model.

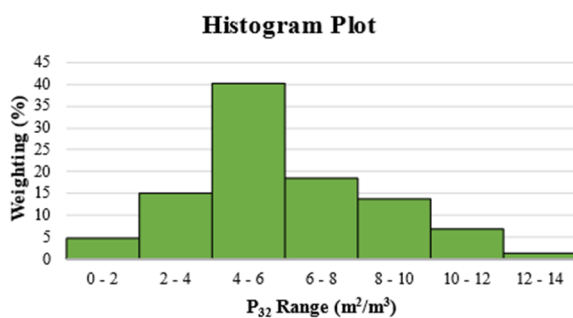


Figure 15 Histogram of P_{32} parameter from boreholes, Continuous Model.

3.6 Granulometric Curves

Granulometric curves were generated using the algorithm Fragmentation Grid (named Sybil Frac) of FracManTM. This method consists of subdividing the volume of interest with a tridimensional grid defined by the user. The minimum volume of the grid is considered as a single cell. In addition, the algorithm identifies

the discontinuities that cross the grid. Those cells that are touched by a discontinuity are characterized like a unitary element conformed by 1 cell. Once all fractures are processed inside the grid and the unitary elements are defined, the remaining cells join, conforming complex blocks. The software compiles the information of all complex blocks and prints a statistical analysis. Figure 16 gives a representative example of the algorithm in a two-dimensional plane, as can be seen, blue cells are the unitary elements crossed by fractures, and purple cells constrain bigger blocks and are limited by blue cells.

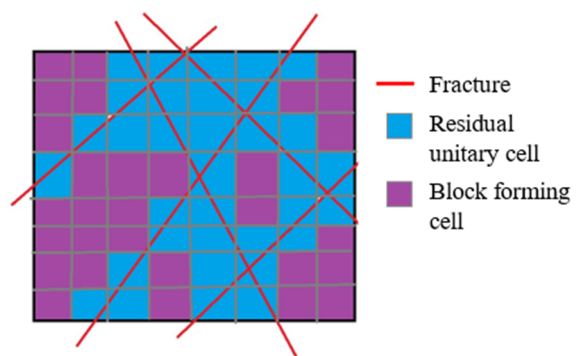


Figure 16 Scheme of Sybil Frac algorithm.

It is important to highlight that the results of this procedure depend on the spacing of the grid, and it is recommended to use a cell size of about 25% of the mean fracture spacing (Elmo et al., 2014). Hence, applying a thinner grid allows us to better identify the real volume of blocks formed by fracture intersections; nevertheless, this leads to slower processing and longer analysis times. So, it is necessary to establish a correlation between evaluation box size, fracture spacing, and grid size.

4 RESULTS AND DISCUSSION

In this chapter, only the results related to fragmentation are presented based on the applied methodology, since the input data was already introduced in Chapter 3. These results seek to answer the secondary objective of this study, which consists of estimating the rock mass fragmentation and evaluating the influence of fracture persistence in its estimation.

The effect proposed by Cai et al. (2004) indicates that the persistence of a fracture set has

an impact on the equivalent block volume according to the observation scale of a rock mass to be evaluated, and consequently, its fragmentation.

The evaluation of granulometric curves was developed according to the ranges of P_{32} identified in the histograms of Figure 14 and Figure 15 to the Discontinuous and Continuous Models, respectively. These histograms were generated from the compound analysis of digital mapping and core logging.

The P_{32} mean value of each range was considered to model a specific DFN in a box of 40 m sides. Then the evaluation of fragmentation was considered through different scale boxes of 3 m, 5 m, 10 m, and 20 m per side. Each evaluation scale considers at least 2 cubes distributed aleatory inside the DFN model. Moreover, to evaluate the persistence effect together with the evaluation scale, the above sequence is applied to Discontinuous and Continuous DFN models to compare its results.

Table 15 and Table 16 present the P_{32} estimations of each discontinuity set used to model Discontinuous and Continuous DFN Models, respectively.

Table 15 P_{32} Parameter for the Discontinuous Model

Global P_{32} (m^2/m^3)	P_{32} Parameter (m^2/m^3)			
	Set 1	Set 2	Set 3	Set 4
1	0.52	0.17	0.15	0.17
3	1.55	0.50	0.45	0.51
5	2.59	0.83	0.74	0.84
7	3.62	1.16	1.04	1.18
9	4.66	1.49	1.34	1.52
11	5.69	1.82	1.63	1.86
13	6.73	2.15	1.93	2.19

Table 16 P_{32} Parameter for the Continuous Model

Global P_{32} (m^2/m^3)	P_{32} Parameter (m^2/m^3)			
	Set 1	Set 2	Set 3	Set 4
1	0.49	0.18	0.15	0.19
3	1.47	0.53	0.44	0.56
5	2.45	0.88	0.73	0.94
7	3.43	1.24	1.02	1.31
9	4.41	1.59	1.32	1.68
11	5.39	1.95	1.61	2.06
13	6.37	2.30	1.90	2.43

As it was indicated in the proposed methodology, each granulometric curve is weighted according to the frequency observed in the histograms, then a mean granulometric curve is obtained. Figure 17 shows an example of the weighting process realized in a 10 m size cube of the Continuous Model.

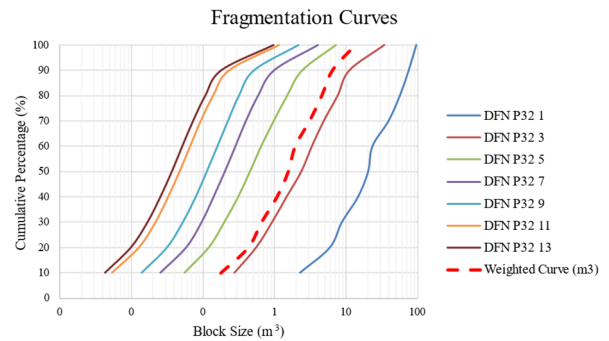


Figure 17 Fragmentation Curves in 10 m Box scale, the Continuous Model.

The following results show the weighted granulometric curves estimated for every observation scale. Figure 18 indicates the analysis of the Discontinuous DFN Model, while Figure 19 shows the results of the Continuous DFN Model.

A first reading of the results indicates that a higher evaluation scale implies a coarser granulometry. This effect is observed both for the Discontinuous Model and the Continuous Model. However, the estimation of P_{80} passing

in the Discontinuous Model range from 12.3 m³ (3 m box) to 2131 m³ (20 m box). On the other hand, the results of the Continuous Model range between 1.2 m³, 2.7 m³, 6.6 m³, and 8.0 m³, for 3 m, 5 m, 10 m, and 20 m evaluation scales, respectively.

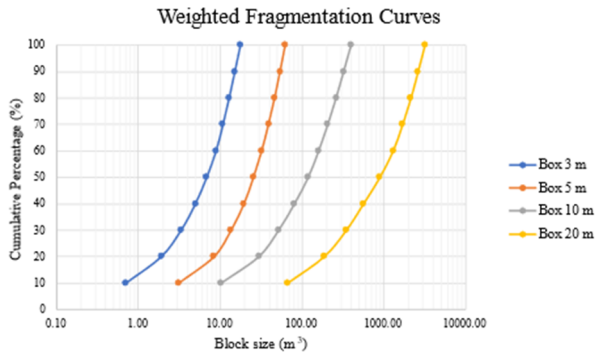


Figure 18 Weighted Fragmentation Curves Discontinuous Model.

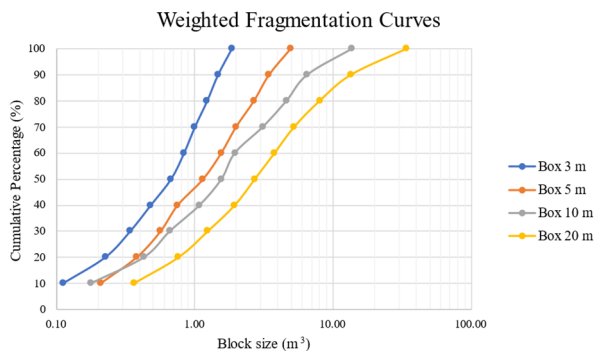


Figure 19 Weighted Fragmentation Curves Continuous Model.

Some historical estimations of fragmentations conducted for the Chuquicamata Underground Mine were made by Barindelli et al. (2018) who estimated P₈₀ values for UGTB QIS between 1.0 m³ to 1.93 m³, applying an analytical methodology that considers fracture frequency from core logging and then transformed to Joint Volumetric (J_v) and Block Volume (V_b) parameters defined by Palmström (2005). Also, Guajardo & Russo (2021) include in their results P₈₀ values of 1.4 m³ for UGTB QIS in MBC N01-S01 at 20 m height extraction. It must be considered that the latter result has a hybrid approach of DFN-BCF focused on secondary fragmentation. Moreover, Pereira et al. (2024) estimated a mean P₈₀ passing of 1.85 m³ according to the record of presential granulometric mapping in draw points between

20 m to 40 m high of in situ extraction in MBC N01-S01.

The comparison between the obtained results and the historical values show that the Discontinuous Model gives significantly higher values for all evaluation scales, while the results reported in the Continuous Model show values within expectations, specifically, the 3 and 5 m observation scales, which are consistent with the magnitude of historical data.

Table 17 Passing P₈₀ (m³) for the Discontinuous Model

Global P ₃₂ (m ² /m ³)	P ₈₀ (m ³) Box Size Scale			
	3 m	5 m	10 m	20 m
1	24.6	97.7	729.2	5969.4
3	19.1	68.6	552.4	4747.9
5	14.3	40.5	163.5	1226.2
7	2.3	30.8	10.6	21.2
9	1.5	4.7	1.1	1.5
11	0.9	1.9	0.3	0.4
13	1.9	0.9	0.6	0.2

Table 18 Passing P₈₀ (m³) for the Continuous Model

Global P ₃₂ (m ² /m ³)	P ₈₀ (m ³) Box Size Scale			
	3 m	5 m	10 m	20 m
1	11.5	23.4	56.8	124.3
3	3.0	7.1	7.5	7.9
5	0.3	0.9	1.5	1.8
7	0.4	0.5	0.6	0.7
9	0.2	0.2	0.3	0.4
11	0.1	0.2	0.1	0.2
13	0.1	0.2	0.1	0.1

A more detailed review of the results can be found in Table 17 and Table 18, where the P_{80} passing of each granulometric curve generated for all ranges of P_{32} is indicated in the Discontinuous and Continuous Models, respectively. With respect to these results, it is indicated that there is a trend of increase in the P_{80} value as the P_{32} decreases, while, for the same volumetric intensity the scale effect shows slight variability evidence of P_{80} , excepting the evaluations of 9, 11, and 13 P_{32} values.

Nevertheless, the magnitudes of the calculated results in Table 17 are higher than those observed for the Continuous Model (Table 18). These results are explained by the presence of rock bridges, which result in a decrease of the fracture intensity. This leads to mega blocks forming and, therefore, the larger the observation scale, the bigger the mega blocks formed. While the Continuous Model is just controlled by the fracture spacing (intensity) and the orientation of sets.

Consequently, the magnitude and influence of rock bridges on the fragmentation, as well as the observation scale, are significant.

5 CONCLUSION AND RECOMENDATIONS

The proposed methodology in this work allows the establishment of a strategy for mapping, analysis, and calibration of DFN models, based on high-resolution digital mapping in underground mining combined with core logging as input data. It is recommended to replicate this method in other sectors of interest in Chuquicamata Underground Mine to amplify the database, identify the structural systems, and differentiate clusters of intensity and orientation by UGTB models and Structural Domain.

The Terzaghi Adjustment Factor (TAF), allowed to integrate and compare the core logging data with the DTM mapping. This factor combines the need to adjust theoretical geotechnical estimations to the rock mass variability. The authors recommend continuing with the analysis of this factor by applying different dispersion levels to the fracture sets orientation, including more trends of P_{10} evaluation, and applying

different criteria of DFN modelling, such that could be differentiated the influence of the variables in the calibration of TAF.

Additionally, the results were coherent with the expected assumption about the influence of fractures persistence on the fragmentation. However, the observation scale effect in models with a constant intensity is not defined with clarity.

Unfortunately, it was not possible to define a more specific correlation between the included variables and the results since this was not included in the scope of the initial study. Nevertheless, new hypotheses and challenges are raised for future research. So, a continuation of these studies is recommended, to determine the correlations between the persistence, the observation scale, the connection in fracture networks, and the presence of rock bridges with the rock mass fragmentation. It is also proposed to estimate through laboratory test the shear and tensile strength of the main block-forming fractures, as well as the integration of geological rock blocks mapping in draw points to understand the process of rock mass disassembling.

Integrating this analysis with numerical models could lead to a better understanding of the propagation and connection between joint systems with the fragmentation under dynamic conditions of caving.

ACKNOWLEDGEMENT

The authors would like to express their gratitude to the GRMD management of Chuquicamata, Codelco Chile, for authorizing the publication of this work. And to Alonso Figueroa for his time, support, and enthusiastic conversations.

REFERENCES

- ADAM Technology (2024). 3DM Analyst Mine Mapping Suite, Measurement Camera Calibration and Block Adjustment Software v 2.3.4.
- Barindelli, G., Harrison, D., López, S. & Constanzo, H. (2018). Estimación de la Frecuencia de Fracturas y GSI Sector Macrobloques N4 al N7 y S4 al S5 Lift 01. Superintendencia Planificación Minería Subterránea, División Codelco Norte, Codelco Chile: GRMD-SPMS-INF-007/2018. (Unpublished).

- Barton, N., Lien, R. & Lunde, J. (1974). Engineering classification of rock masses for design of tunnel support. *Rock Mechanics*, 6(4): 189-236.
- Cai, M., Kaiser, P., Uno, H., Tasaka, Y. & Minami, M. (2004). Estimation of rock mass deformation modulus and strength of jointed hard rock masses using the GSI system. *International Journal of Rock Mechanics and Mining Sciences*. 41. 3-19. 10.1016/S1365-1609(03)00025-X.
- CloudCompare (2023). Version 2.13 [GPL software]. Retrieved from <http://www.cloudcompare.org/>.
- Codelco Norte (2009). Caracterización Geotécnica Estructural, Proyecto Mina Subterránea Chuquicamata, Delineamiento para Ingeniería Básica. Informe Interno, Área de Caracterización Geotécnica Estructural, Superintendencia de Geotecnia Línea Sulfuros, Dirección de Geotecnia, División Codelco Norte, Codelco Chile: 180 pp. Chuquicamata. (Unpublished).
- Dershowitz, W. S. & Herda, H. H. (1992). Interpretation of fracture spacing and intensity. In Proceedings, 33rd U.S. Symposium on Rock Mechanics, 3-5 June 1992, Santa Fe. Rotterdam: Balkema, pp. 757-766.
- Díaz, M., López, S. & Aguirre, R. (2015). Entrega Parámetros Geomecánicos Proyecto Mina Chuquicamata Subterránea. Nota Interna SUP-GEOT-N°059/2015, Junio de 2015. Superintendencia de Geotecnia, Gerencia de Recursos Mineros y Desarrollo, División Chuquicamata de Codelco-Chile. (Unpublished).
- Divasto, C. (2018). Metodología para construcción de Modelos Discretos de Fracturas en minería a Rajo Abierto, Codelco División Andina, V Región, Chile. Tesis para optar al título de Geólogo, Departamento de Ciencias Geológicas, Universidad Católica del Norte, Antofagasta, Chile.
- Elmo, D., Rogers, S., Stead, D. & Eberhardt, E. (2014). Discrete fracture network approach to characterize rock mass fragmentation and implications for geomechanical upscaling, *Mining Technology*, vol. 123, no. 3, pp. 149-161.
- Espinoza, R. (2018). Variabilidad especial de la Resistencia de la roca intacta (IRS) y del índice geológico de resistencia (GSI) en las unidades geotécnicas básicas de mina Chuquicamata. Región de Antofagasta, Chile. Memoria para optar al Título de Geólogo, Departamento Ciencias de la Tierra, Universidad de Concepción, Concepción, Chile.
- Golder (2021). FracMan version 8.0 Manual. Golder Associates (UK) Ltd.
- González, P. (2022). Sistema de Fotogrametría Digital Interior Mina Tecnología ADAM. Derk Ingeniería y Geología, Codelco Chuquicamata. (Unpublished)
- Guajardo, C. & Russo, A. (2021). Reporte Final de la Estimación de Fragmentación para los Macrobloques del Primer y Segundo Nivel de Minera Chuquicamata Subterránea. SRK Consulting (Chile) SpA, SRK 01-2400-01.
- Guajardo, C., Jakubec, J., Esterhuizen, E., Pichuante, H. & Thomas, A. (2022). The Discrete Fracture Network-Block Caving Fragmentation hybrid method: A new tool to assess fragmentation of block caving mining projects, in Y Potvin (ed.), Caving 2022: Proceedings of the Fifth International Conference on Block and Sublevel Caving, Australian Centre for Geomechanics, Perth, pp. 927-938.
- Hekmatnejad, A., Saavedra, C. O., & Crespín, B. (2022). Presentation of the Universal Discontinuity Index (Udi) System and its Application to Predict the Geometry of Over-Excavation Along a Tunnel at El Teniente Mine. *Engineering Geology*, Volume 311, 106901, ISSN 0013-7952.
- Kuppusamy, V. (2022). Application of Discrete Fracture Networks (DFN's) to the design of benches in an open pit mine in South Africa. The Evolution of Geotech – 25 Years of Innovation, 1st Edition. ISBN 978-1-032-03645-8.
- LaPointe, P. R. (2002). Derivation of parent fracture population statistics from trace length measurements of fracture populations. *International Journal of Rock Mechanics and Mining Science*, v. 39, p. 381-388.
- Maptek (2019). PointStudio 8.1.1. Point cloud processing, modelling and analysis tools for mining and industrial survey v 8.1.1.12349.
- Mauldon, M. & Dershowitz, W. (2000). A Multi-Dimensional System of Fracture Abundance Measures. Geological Society of America Annual Meeting. Reno, Nevada.
- Ortiz, F. (2019). Metodología de Construcción de Modelos DFN, Para Determinación de Fragmentación In Situ en el Yacimiento Río Blanco. *Journal of Mining Engineering and Research* 1, no. 1: 55-61.
- Palmström, A. (2005). Measurements of and correlations between block size and rock quality designation (RQD). *Tunnelling and Underground Space Technology*, Volume 20, Issue 4, Pages 362-377, ISSN 0886-7798, <https://doi.org/10.1016/j.tust.2005.01.005>.
- Pereira, J., Divasto, C. & Barindelli, G. (2024). Informe Semestral Fragmentación Sectores MB S02-S03, MB N02-N03 y MBC N01-S01, a diciembre de 2023 - Mina Chuquicamata Subterránea. Informe DERK-SEG-FRAG-INF-001-2024, preparado por Empresa DERK Ingeniería y Geología Ltda. - Contrato N°4600022833, para la Superintendencia de Estudios Geomecánicos, División Chuquicamata de Codelco-Chile. (Unpublished)

- Push, R. (1995). *Rock Mechanics on a Geological Base*. Elsevier, ISBN 008054066X, 51-54.
- Rocscience (2019). Dips v7.016, Copyright © 1989-2019 Rockscience Inc. <http://www.rockscience.com>.
- Rogers, S., Moffitt, K. & Kennard, D. (2006). Probabilistic tunnel and slope block stability using realistic fracture network models, in DP Yale (ed.), *Proceedings of the 41st US Rock Mechanics Symposium*, American Rock Mechanics Association, Alexandria.
- Rogers, S., Chorley, D., Pesendorfer, M., Zawadski, W. & Greer, S. (2009). Hydrogeological characterization and conceptual DFN flow modelling of slope pressures within the Diavik diamond mine, NWT, in J Read (ed.), *Proceedings of the International Symposium on Rock Slope Stability in Open Pit Mining and Civil Engineering*, University of the Andes, Santiago.
- Rogers, S., Elmo, D., Webb, G. & Catalan, A. (2010). A discrete fracture network based approach to defining in situ, primary and secondary fragmentation distributions for the Cadia East panel cave project, in Y Potvin (ed.), *Proceedings of the Second International Symposium on Block and Sublevel Caving*, Australian Centre for Geomechanics, Perth, pp. 425–440.
- Rogers, S. F., Elmo, D., Webb, G. & Cristián Guajardo Moreno. (2016). DFN Modelling of Major Structural Instabilities in a Large Open Pit for End of Life Planning Purposes. Paper presented at the 50th U.S. Rock Mechanics/Geomechanics Symposium, Houston, Texas.
- Siña, A., Maksaev, V., Munizaga, F. & Vivanco, M. (2005). Chuquicamata Subterráneo, raíces hipógenas de un pórfido gigante de Cu-Mo generado por sucesivos eventos hidrotermales sobreimpuestos: evidencias geológicas y geocronológicas. División Codelco Norte, Codelco Chile (Inédito): 170 pp. Chuquicamata.
- Terzaghi, R. D. (1965). Sources of error in joint surveys. *Geotechnique*, 15(3), 287-304.
- Zeeb, C., Gomez-Rivas, E., Bons, P. & Blum P. (2013). Evaluation of sampling methods for fracture network characterization using outcrops. *AAPG Bulletin*; 97 (9): 1545–1566.